

Reactivity of formic acid (HCOOH) with H atoms on cold surfaces of interstellar interest

Henda Chaabouni, Saoud Baouche, Stephan Diana, Marco Minissale

► **To cite this version:**

Henda Chaabouni, Saoud Baouche, Stephan Diana, Marco Minissale. Reactivity of formic acid (HCOOH) with H atoms on cold surfaces of interstellar interest: Reactivity on cold surfaces. Astronomy and Astrophysics - A&A, EDP Sciences, 2020, 636, pp.A4. 10.1051/0004-6361/201936411 . hal-02564728

HAL Id: hal-02564728

<https://hal.archives-ouvertes.fr/hal-02564728>

Submitted on 6 May 2020

HAL is a multi-disciplinary open access archive for the deposit and dissemination of scientific research documents, whether they are published or not. The documents may come from teaching and research institutions in France or abroad, or from public or private research centers.

L'archive ouverte pluridisciplinaire **HAL**, est destinée au dépôt et à la diffusion de documents scientifiques de niveau recherche, publiés ou non, émanant des établissements d'enseignement et de recherche français ou étrangers, des laboratoires publics ou privés.

Reactivity of formic acid (HCOOH) with H atoms on cold surfaces of interstellar interest

Henda Chaabouni¹, Saoud Baouche¹, Stephan Diana¹, and Marco Minissale²

¹ LERMA, Université de Cergy-Pontoise, Observatoire de Paris, PSL Research University, Sorbonne Université, UMR 8112, CNRS, 5 mail Gay Lussac, 95000 Cergy-Pontoise, France
e-mail: henda.chaabouni@cyu.fr

² Aix-Marseille Université, CNRS, PIIM, Marseille, France

Received 30 July 2019 / Accepted 13 January 2020

ABSTRACT

Context. Formic acid (HCOOH) is the simplest organic carboxylic acid in chemical synthesis and the significant species in interstellar chemistry. HCOOH has been abundantly detected in interstellar ices, dense molecular clouds and star-forming regions.

Aims. Laboratory hydrogenation experiments of HCOOH molecules with H atoms were performed with two cryogenic ultra-high vacuum devices on amorphous solid water ices, and highly oriented pyrolytic graphite surfaces. The aim of this work is to study the reactivity of HCOOH molecules with H atoms at low surface temperature 10 K, low surface coverage of one monolayer to three layers, and low H-atom flux of about 3.0×10^{12} molecule $\text{cm}^{-2} \text{s}^{-1}$.

Methods. HCOOH and H beams were deposited on cold surfaces held at 10 K, and the condensed films were analyzed by in-situ Reflection Absorption InfraRed Spectroscopy and temperature programmed desorption (TPD) mass spectrometry technique by heating the sample from 10 to 200 K.

Results. Using the temperature programmed during exposure desorption technique, we highlight the possible dimerization of HCOOH molecules at low surface temperatures between 10 and 100 K. In our HCOOH+H experiments, we evaluated a consumption of 20–30% of formic acid by comparing the TPD curves at m/z 46 of pure and H-exposed HCOOH ice.

Conclusions. The hydrogenation HCOOH+H reaction is efficient at low surface temperatures. The main products identified experimentally are carbon dioxide (CO₂) and water (H₂O) molecules. CO bearing species CH₃OH, and H₂CO are also detected mainly on graphite surfaces. A chemical surface reaction route for the HCOOH+H system is proposed to explain the product formation.

Key words. astrochemistry – methods: laboratory: molecular – techniques: spectroscopic – ISM: atoms – ISM: molecules – atomic processes

1. Introduction

Formic acid (HCOOH), the simplest organic acid, is thought to play a major role both in atmospheric and interstellar environments, as well as human body (Cao et al. 2014) as intermediate in chemical synthesis of organic molecules and pre-biotic species. With its derivative formate group (–(C=O)OH), formic acid is considered as the basis compound for the formation of more complex carboxylic acids (RCOOH) and biomolecules used by life on Earth, including amino acids, glycine, and DNA bases (Pilling et al. 2011). HCOOH is also the smallest organic acid which has been detected in cold dark interstellar clouds L134 N with a relative abundance of 10^{-10} with respect to H₂ (Irvine et al. 1990). It has been observed in the gas phase towards high- and low-mass star-forming regions (Woods et al. 1983; Bisschop et al. 2007a; Lefloch et al. 2017), and towards L1544 (Vastel et al. 2014) with a fractional gas-phase abundance $[\text{HCOOH}]/[\text{H}_2] = 10^{-11} - 10^{-9}$. It has also been observed toward hot molecular cores in Orion Kleinmann-Low (KL) region of star formation at brightness temperatures between 100 and 200 K, where icy mantles undergo sublimation or destruction (Liu et al. 2001). HCOOH has been abundantly identified in interstellar ices before the onset of star formation (Knez et al. 2005; Keane et al. 2001) with abundances of 2–10% with respect to solid H₂O (Knez et al. 2005). The earlier tentative

detection of HCOOH towards the high-mass young stellar object (NGC 7538:IRS9) suggests that formic acid is a general component of ices in the vicinity of embedded high-mass young stellar objects (Schutte et al. 1999). In dense molecular clouds, solid HCOOH is likely mixed with abundant species in the ice like H₂O, CO, CO₂, and CH₃OH. Moreover, formic acid together with methanol (CH₃OH) and formaldehyde (H₂CO) are considered to be the most abundant complex molecules detected in protoplanetary disks so far. Recently, Favre et al. (2018) reported the first detection of HCOOH towards the TW Hydrae protoplanetary disk. The observations with the Atacama Large Millimeter/submillimeter Array (ALMA) have shown the trans-HCOOH 6(1,6)–5(1,5) transition at 129 GHz for the lower energy formic acid conformer (Lopes et al. 2018), and the measurements revealed a disk-average gas phase trans-HCOOH column density of $2-4 \times 10^{12} \text{ cm}^{-2}$, as large as that of methanol CH₃OH. Cis and trans-HCOOH planar isomer conformers refer to the relative position of the two H atoms in the molecule with respect to C–O bond (Szymafiski & Gillan 1996; Lopes et al. 2018). The radioastronomical observations acquired with the IRAM 30 m telescope revealed the detection of HCOOH even in the comet C/2013R1 (Lovejoy) of planetary system (Makochekanwa et al. 2014). A recent astrochemical model of Skouteris et al. (2018) shows a new gas-phase scheme of reactions for the formation of formic acid involving ethanol (CH₃CH₂OH) as a parent molecule.

Whereas, the gas-grain chemical simulations of Garrod et al. (2008) assumed that HCOOH is formed by the recombination of HCO and OH radicals on the grain surfaces. This assumption was recently contradicted by the model of Vasyunin et al. (2017), who considered that the reaction between HCO and OH is inefficient because both reactants do not diffuse in the surface at the low temperatures of prestellar cores. The authors thus suggest that HCOOH is formed through the radiative association reaction $\text{HCO}^+ + \text{H}_2\text{O}$, and then accumulated in the ice via gas accretion. Formic acid is predominantly formed in dense interstellar clouds through surface reactions on grains. In the laboratory, HCOOH has been formed on cold surfaces (Ioppolo et al. 2011) by the co-deposition of H atoms and CO:O₂ mixtures through the hydrogenation of the HO-CO complex. This can confirm the presence of formic acid in dense cold clouds, at the beginning of the warm-up phase of a protostar. Pure HCOOH ice as well as HCOOH-H₂O and HCOOH-CH₃OH ice matrices have been widely characterized by infrared spectroscopy in previous works (Bisschop et al. 2007a; Bennett et al. 2011). Whereas HCOOH dimers and their different cis and trans conformers were recently studied experimentally by infrared spectroscopy in nitrogen matrix, and theoretically by ab-initio calculations (Lopes et al. 2018). The heat of dimerization of formic acid by FTIR, reported in an early work (Henderson 1987) is $\Delta H_D = (-48.0 \pm 0.4) \text{ kJ mol}^{-1}$. The reactivity of formic acid with neutral atomic hydrogen was studied theoretically (Cao et al. 2014) and experimentally (Bisschop et al. 2007b; Cao et al. 2014) in the literature. Cao et al. (2014) have studied the reaction $\text{HCOOH} + \text{H}$ in a rare-gas Kr matrix and characterized the isolated radical products using infrared spectroscopy and ab-initio quantum chemical calculations. Their theoretical studies have suggested three possible channels for the $\text{HCOOH} + \text{H}$ reaction: (i) reaction with the oxygen atom of the hydroxyl group ($-\text{OH}$) of HCOOH leading to H₂O formation with HCO radical, (ii) reaction with the oxygen atom of the carbonyl group ($-\text{C}=\text{O}$) leading to the formation of diols $\text{HC}(\text{OH})_2$, and (iii) reaction with the carbon atom of carbon-hydrogen group ($-\text{CH}$) leading to the formation of the radical H₂COOH. See reactions (1), (2), and (3), respectively:



The computational energetic predictions revealed, firstly, the formation of an intermediate radical trans-H₂COOH (*m/z* 47) through the reaction (3), which converts to the more stable radical isomer trans-cis-HC(OH)₂ diol via hydrogen atom tunneling on a timescale of hours at 4.3 K. This simplest and lowest energetic diol, identified in their work as the final product, is expected to be very reactive, and further reaction channels are of particular interest. Previous cryogenic laboratory experiments performed in Leiden group of H-atom addition to pure HCOOH ice at 15 K on cold surfaces (Bisschop et al. 2007b) did not result in detectable reaction products within the experimental sensitivity of their set-up. In their work performed in the multilayer regime, the authors exposed thick films of pure HCOOH ice of 20 layers and a mixed (HCOOH+H₂O) film of 40 layers on golden substrate with H-fluence of $7 \times 10^{14} \text{ molecule cm}^{-2} \text{ s}^{-1}$.

In this paper, we experimentally study the reactivity of HCOOH molecules adsorbed on graphite and amorphous water ice surfaces with a typical H atom-flux of $3.0 \times 10^{12} \text{ molecule cm}^{-2} \text{ s}^{-1}$, at low surface temperatures of 10 K and low surface coverage of HCOOH ice varying from one to three

layers. We used two cryogenic setups with different configurations of molecular and atomic beam lines for the deposition of the reactants on the cold surfaces. The two setups allow us to study the effect of various substrates (gold, carbonaceous graphite and water ice) on the reaction $\text{HCOOH} + \text{H}$ by using different experimental methods for the identification of the species adsorbed and desorbed from the surfaces, mainly Reflection Absorption InfraRed Spectroscopy (RAIRS), temperature programmed desorption (TPD), and temperature programmed during exposure desorption (TP-DED). This paper is organized as follows: Sect. 2 explains the experimental methods; Sect. 3 focuses on the data analysis for the dimerization and the reactivity of HCOOH with H atoms; Sect. 4 is open for the discussion of the experimental results; and Sect. 5 presents the astrophysical implications and summarizes the main conclusions of this work.

2. Experimental

The experiments were performed with the FORMation of MOlecules in the InterStellar Medium (FORMOLISM) and Vers de NoUvelles Syntheses (VENUS) apparatus located in LERMA-Cergy laboratory. The setups are dedicated to study the reactivity of molecules and atoms on surfaces of astrophysical interest as well as the formation of simple and complex organic molecules, under temperature and pressure conditions similar to those encountered in the ISM. FORMOLISM apparatus is well-described in previous papers (Amiaud et al. 2007; Congiu et al. 2012). It is composed of an ultra-high vacuum chamber (UHV) stainless steel chamber with a base pressure lower than 10^{-11} mbar. The sample holder located in the main chamber is thermally connected to a cold finger of a closed-cycle He cryostat. It is made of a 1-cm-diameter copper block covered with a highly oriented pyrolytic graphite (HOPG, ZYA-grade) slab. The temperature of the sample is measured in the range of 10–700 K by a calibrated silicon diode clamped to the sample holder. Before starting the experiments, the surface of the graphite substrate is heated from 10 to 700 K with a small heating rate of 2 K per minute by maintaining the pressure in the main UHV chamber close to 10^{-9} – 10^{-10} mbar. The surface is then cooled down to 10 K for the exposure of the reactants. This operation is practiced to clean the surface of the graphite substrate from any volatile contaminants (CO, CO₂, CH₄...) that might be trapped in the defects and modify the structure of the surface. This allows as to have reproducible profiles for the infrared and the TPD spectra of the studied molecules. The UHV chamber of FORMOLISM set-up is also equipped with an amovable quadrupole mass spectrometer (QMS) of mass spectra ranging from 1 to 100 atomic mass unit (AMU) with a Channeltron detector. It can be rotated and placed in front of each beam line to characterize the chemical gas composition of the HCOOH and the H beams. It can also be faced to the surface of the sample holder at 1 cm distance to perform TPD measurements. During the warm-up phase of the sample from 10 to 200 K, the species desorbing from the surface into the gas phase are detected with the QMS by their mass-to-charge ratio (*m/z*). The VENUS setup described in recent papers (Minissale et al. 2019; Nguyen et al. 2018) is composed of a main UHV chamber with a low pressure of 10^{-10} mbar, where a gold-coated copper sample holder is placed in the central position of the main chamber and thermally connected to a Helium liquid closed cycle cryocooler. This main chamber itself is linked to an intermediate UHV chamber through five diaphragms of 3 mm in diameter materializing the direction of five beam-lines aimed to the center of the gold surface. Like

FORMOLISM, VENUS setup is equipped with a QMS and a Fourier transform infrared (FTIR) spectrometer in RAIR configuration using an external mercury cadmium tellurite (MCT) detector cooled with liquid nitrogen. Contrarily to the FORMOLISM setup, the VENUS setup has the advantage of being able to record the infrared spectra in real time during the exposure of the surface to the molecular and atomic beams without moving the sample holder. The chemical components used in this work are liquids HCOOH (Sigma Aldrich Fisher Scientific 98% purity) and H₂O (deionized), which are introduced in pyrex flasks. The H-beam is obtained through the dissociation of H₂ beam with a microwave source. The hydrogen atomic plasma is generated through the microwave discharge within the Surfatron cavity operating at 2.45 GHz. The hydrogen beam dissociation rate is measured by the QMS from H₂ signals during the discharge (ON) and the discharge (OFF) of the microwave source. The value of the dissociation rate varies between 60 and 75%, with an effective microwave power of 60 Watt. The flux of H-atoms coming from the gas phase and hitting the surface is measured from the so-called King and Wells method described in the reference (Amiaud et al. 2007). The estimated H-flux is $(3.7 \pm 0.5) \times 10^{12}$ atom cm⁻² s⁻¹.

For the HCOOH beam, the flux of formic acid molecules is derived from TPD data, and defined as the amount of solid HCOOH that saturates the surface per unit time. The HCOOH-flux value is estimated to 2.6×10^{12} molecule cm⁻² s⁻¹. The chemical composition of the HCOOH beam is checked by placing the QMS in front of the HCOOH beam line. The main cracking pattern ion fragments of gaseous HCOOH are m/z 46 (HCOOH⁺, 26%), m/z 45 (HCOO⁺, 17%), m/z 44 (COO⁺, 4%), m/z 29 (HCO⁺, 20%), m/z 28 (CO⁺, 10%), m/z 18 (H₂O⁺, 13%). During the characterization of the HCOOH beam, the QMS did not detect masses higher than m/z 46.

Amorphous solid water (ASW) ice is grown on top of the gold (or graphite) surface maintained at 110 K, by spraying water vapor from a micro-channel array doser located inside the ultra-high vacuum chamber (UHV). The water vapor was obtained from deionized liquid water purified by several pumping cycles under cryogenic vacuum (Noble et al. 2012). The thickness of the water ice film is 10 layers, where one monolayer unit is defined as 1 ML = 10^{15} molecule cm⁻². For the HCOOH+H experiments, we firstly deposited one to three layers of HCOOH on the surface held at 10 K, and then we exposed the film of formic acid to H beam at the same surface temperature for several exposure times. For comparison, co-deposition experiments of HCOOH and H beams on cold surfaces are also performed using two beam lines simultaneously. After the deposition phase of HCOOH or HCOOH + H films, an infrared spectra were recorded in the mid-infrared region ($4000\text{--}400$ cm⁻¹ or $2.5\text{--}25$ μm) with a spectral resolution of 4 cm⁻¹ and an average number of 400 scans. The TPD method is performed in the 10–200 K temperature range with a linear heating rate of 0.2 K s⁻¹. We also performed TP-DED experiments to study the dimerization of HCOOH on the surface of the sample holder using FORMOLISM setup. The TP-DED technique is well-described in Minissale et al. (2016a), and consists of exposing the sample to the molecular beam (here HCOOH) while slowly reducing the sample temperature from a higher temperature, where the molecules remain in the gas phase, to a lower surface temperature, where they stick on the surface. In these experiments, the QMS (see Fig. 1a) was placed close to the surface in the lower position, between the direction of the beam line and that of the surface, at a specified orientation angle of about 55° relative to the normal to the sample holder, in order to collect the maximum amount of formic acid species

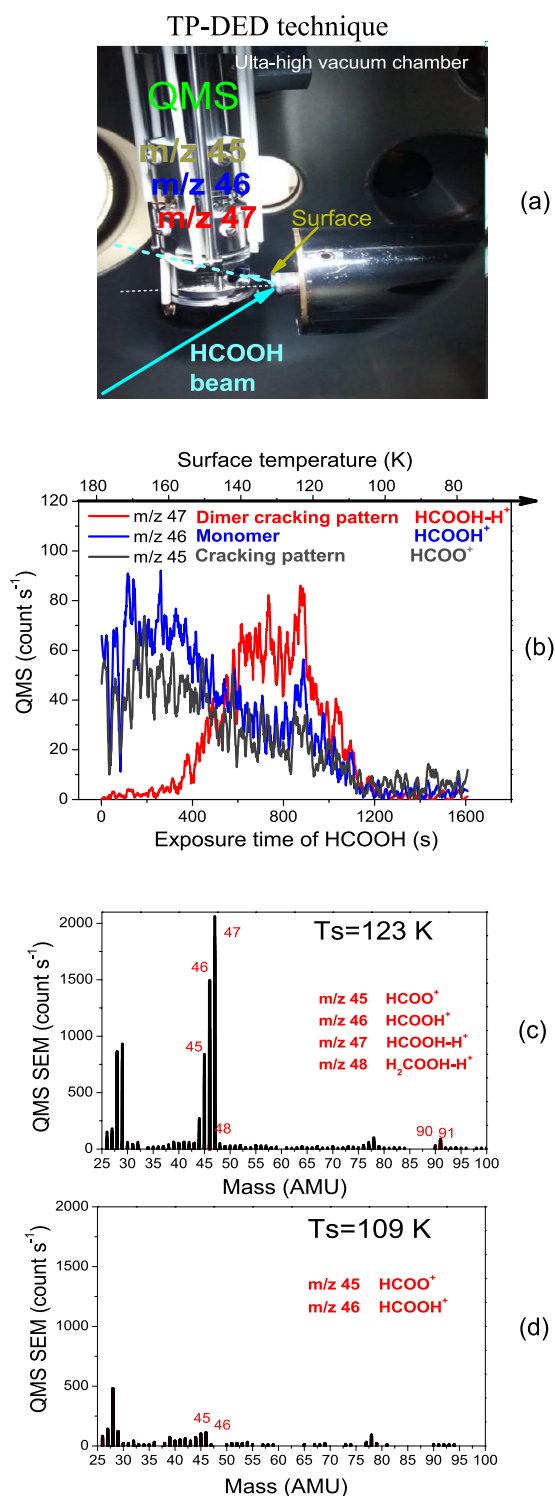


Fig. 1. Description of the dimerization process of HCOOH using FORMOLISM setup. *Panel a:* TP-DED experimental configuration. *Panel b:* QMS signals of m/z 47, m/z 46 and m/z 45 during TP-DED between 180 and 100 K on the gold surface with a small heating rate of 0.033 K s⁻¹. *Panels c and d:* QMS bar mass spectra in the 25–100 AMU range recorded for two surface temperatures at 123 and 109 K.

released from the surface during the exposure of the surface to the HCOOH beam. The species promptly reflected from the surface, or desorbed into the gas phase after thermalization, were continuously measured by the QMS during the linear cooling of the sample from 180 to 100 K, using a small heating rate of 0.033 K s⁻¹.

3. Experimental results

3.1. Dimerization of HCOOH on the gold surface

Figure 1, panel b shows the TP-DED experiments in the 180–100 K range of m/z 45, 46, and 47 during the exposure of a gold sample to the HCOOH beam. For surface temperatures ranging between 180 and 160 K, formic acid molecules (detected at m/z 45 HCOO^+ and m/z 46 HCOOH^+) do not stick on the surface, promptly returning to the gas phase. For temperatures varying from 160 to 145 K, the signal at m/z 46 decreases indicating that HCOOH starts to stick efficiently on the surface. On the other hand, m/z 47 starts to increase. Such signal is likely result of the HCOOH dimers desorption that is cracked in the QMS head (H_2COOH^+ , m/z 47). At 145–125 K, the signal of mass m/z 47 reaches a maximum of 80 count s^{-1} , while those of m/z 46 and m/z 45 remain at 30 count s^{-1} . As the temperature of the surface decreases to 100 K, the signals of m/z 47, m/z 46, and m/z 45 drop and reach the minimum values, because both monomers and dimers of formic acid molecules condensate on the surface, and their adsorption rate exceeds that of their desorption. Figure 1 panels c and d confirm our observations in Fig. 1, panel b by showing the QMS bar lines in count s^{-1} of the partial pressure in the UHV chamber as a function of the m/z in atomic mass unit (AMU), during the surface exposure to the HCOOH beam, at two surface temperatures of 123 K and 109 K, respectively. At $T_s = 123 \text{ K}$, Fig. 1, panel c shows the cracking patterns of the HCOOH monomer and dimer reflected from the surface, mainly at m/z 45, m/z 46 and m/z 47, and probably traces at m/z 48, 90 and 91. These masses are less abundant at $T_s = 109 \text{ K}$ in Fig. 1, panel d when HCOOH molecules condensate on the surface. Figure 2 shows the cycle complex structure ($\text{HCOOH} - \text{HCOOH}$) of formic acid dimer, which can be formed on the surface through the association of two adsorbed HCOOH molecules linked together by double hydrogen bond ($-\text{O}\cdots\text{H}$) modeling the noncovalent interaction between two HCOOH molecules. The average hydrogen bonding ($-\text{O}\cdots\text{H}$) energy is 20 kJ mol^{-1} or 0.2 eV . A control experiment was performed by rotating the QMS face to the beam line of HCOOH in order to analyze the chemical composition of the HCOOH beam, by measuring the signals of the cracking patterns of the species coming from the beam. In this case, no signals of m/z 47 and other higher masses are provided by the QMS, meaning that the dimerization of HCOOH cannot occur in the beam at room temperature for very low HCOOH vapor pressure of 10^{-5} – 10^{-8} mbar. The sharp peak in Fig. 1, panel b observed for masses 47, 46 and 45 of formic acid at a specific surface temperature 123 K has not been observed in the signals of other masses (44, 32, 31, 29, 28, 18, and 17) used in this experiment. In addition, a similar TP-DED experiment of HCOOH performed on a graphite (HOPG) substrate showed similar sharp peaks for the same masses 47, 46 and 45 at the same range of temperature 123–127 K. This leads us to consider that this peak is not a noise or a parasite signal caused by uncommon dysfunction of the QMS, but a real signal of the maximum desorption of formic acid dimers upon formation on the surface at 123 K from the adsorbed neighboring monomers. This means that the residence time of the newly formed dimer (HCOOH-HCOOH) molecules on the surface at 123 K remains shorter than the lifetime of the adsorbed HCOOH monomers, probably because of the local heat released from the exothermic dimerization of HCOOH on the surface (Henderson 1987). The dimerization excess energy would briefly heat the sample (Hellebust et al. 2007) at this surface temperature and provoke

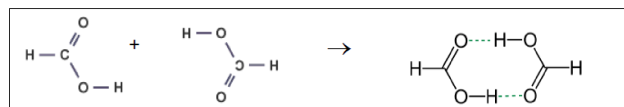


Fig. 2. Chemical structure of the formic acid dimer.

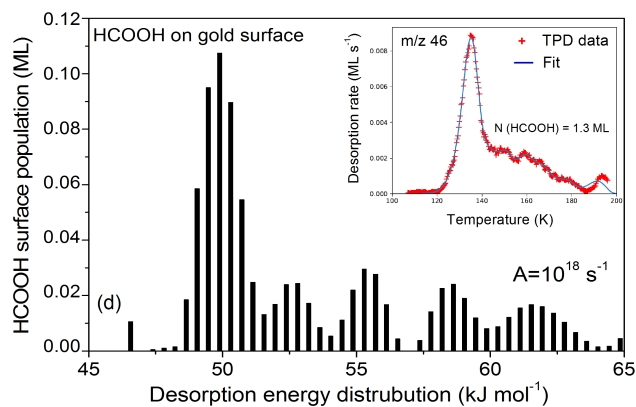
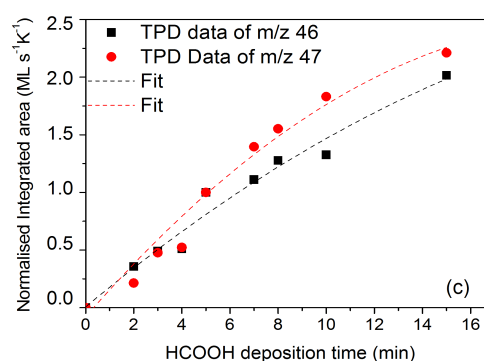
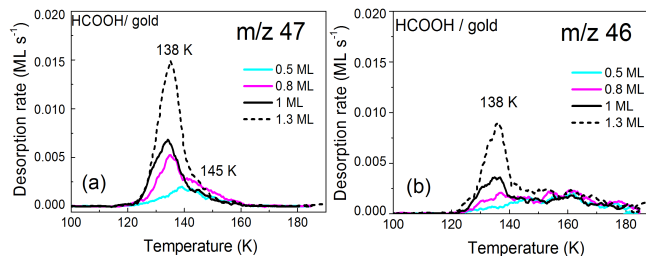


Fig. 3. Thermal desorption results of HCOOH from gold surface. *Panel a and b*: desorption rates of HCOOH for m/z 47 and m/z 46 on gold surface; *panel c*: integrated areas below the TPD curves of HCOOH for m/z 47 and m/z 46 as a function of the HCOOH exposure time on gold surface; and *panel d*: surface population of HCOOH as a function of the desorption energy of HCOOH from gold surface for m/z 46. The desorption energy distribution E_i (in kJ mol^{-1}) and the surface population N_i (in ML) are derived from the desorption rate Eq. (4) with the best-fit pre-exponential factor $A = 1 \times 10^{18} \text{ s}^{-1}$. Figure in the inset shows the best fit of the TPD data (m/z 46) of HCOOH on gold surface for an exposure dose $N = \sum_{i=1}^n N_i = 1.3 \text{ ML}$.

the abrupt desorption of the amorphous solid formic acid dimers into the gas phase.

3.2. Adsorption-desorption of HCOOH on the gold surface

The TPD family curves of pure HCOOH pre-deposited on gold surface at 10 K are shown in Fig. 3, panels a and b for m/z 47 and

m/z 46, respectively. For the exposure doses lower than 1 ML, the profiles of the TPD peaks of m/z 46 and m/z 47 are different. The desorption curves of HCOOH (m/z 46) present a large peak at 140–180 K corresponding to the sub-monolayer desorption regime of HCOOH monomer (cis and trans) molecules from the energetic adsorption sites of the golden surface. As the exposure dose increases from 0.5 ML to 1 ML, a second TPD peak grows at 138 K, and continues to increase for 1.3 ML. This peak corresponds to the multilayer desorption regime of HCOOH ice. TPD curves of m/z 47 follow an order zero, where the maximum of the desorption peaks shifts to the lower temperatures from 145 to 138 K with the increasing surface exposure dose of formic acid from 0.5 to 1.3 ML. In Fig. 3c, we see the evolution of the integrated areas below the TPD curves with the HCOOH exposure time. The data are more important for m/z 47 than 46 when the adsorbed formic acid surface density increases and the thickness of the ice grows, favoring therefore the association of HCOOH monomers into dimers.

Using the TPD data of HCOOH on gold surface for m/z 46 and the set of independent Polanyi-Wigner equations described in the paper (Chaabouni et al. 2018), we estimated the desorption energy distribution of HCOOH on gold surface for HCOOH exposure dose $N = 1.3$ ML. Figure 3d shows the desorption energy distribution E_i (in kJ mol^{-1}) of HCOOH as a function of the surface population N_i (in ML) of formic acid molecules adsorbed on the gold substrate. The surface exposure dose N (in ML) of HCOOH molecules is the sum of the surface fraction exposure doses N_i ($N = \sum_{i=1}^n N_i = N_1 + N_2 + \dots$). The desorption parameters (E_i , N_i) are calculated using the Arrhenius desorption rate Eq. (4):

$$r(T) = \sum_{i=1}^n AN_i e^{-E_i/k_B T} = AN_1 e^{-E_1/k_B T} + AN_2 e^{-E_2/k_B T} \dots, \quad (4)$$

where N_i is the surface population of HCOOH molecules desorbing at a surface temperature T (in K) with a desorption energy barrier E_i (in kJ mol^{-1}), A is the pre-exponential factor for desorption (in s^{-1}), and k_B is the Boltzmann constant ($k_B = 1.38 \times 10^{-23} \text{ J K}^{-1}$). The desorption energy distribution (45–65 kJ mol^{-1}) of HCOOH from gold surface shown in Fig. 3d is calculated with the best-fit pre-exponential factor $A = 1 \times 10^{18} \text{ s}^{-1}$ of the m/z 46 TPD data. This range of desorption energies includes the value 55 kJ mol^{-1} (or 6615 K) reported in the work of Burke et al. (2015) for the desorption energy of carboxylic acid (RCOOH) from graphite substrate using a pre-exponential factor $8 \times 10^{17} \text{ s}^{-1}$. We note that the best-fit pre-exponential factor (A) for desorption of HCOOH found in this work is similar to that of formamide ($\text{NH}_2(\text{C}=\text{O})\text{H}$) molecules calculated from graphite surface in a previous paper (Chaabouni et al. 2018). The high value of A is likely to be related to the chemical carbonyl group ($-\text{C}=\text{O}$) of these complex organic molecules.

3.3. Reactivity of HCOOH with H atoms on cold surfaces

3.3.1. HCOOH+H system on graphite (HOPG) surface

The reactivity of HCOOH with H atoms has been performed in the laboratory on the graphite (HOPG) surface using the FORMOLISM setup and two beam lines for HCOOH and H atoms. The experiments consist firstly of depositing 2 ML of HCOOH ice on the HOPG surface held at 10 K, and then exposing the film to the atomic hydrogen beam for 50 min at the same surface temperature. Figure 4 compares the RAIR spectra of the solid HCOOH deposited on the HOPG surface before and after

H atom addition. The RAIR spectrum a of Fig. 4 shows the IR absorption bands of pure (2 ML) solid HCOOH on HOPG, mainly at 1740 cm^{-1} for the stretching vibration mode $\nu_S(\text{C}=\text{O})$, 1397 cm^{-1} for the antisymmetric deformation modes $\delta(\text{OH})$ or $\delta(\text{CH})$, 1237 cm^{-1} for the stretching vibration mode $\nu_S(\text{C}-\text{O})$, and 1080 cm^{-1} for the bending mode $\nu_B(\text{H}-\text{C}-\text{O})$ out of plane representing molecular vibrations oscillating perpendicular to the plane of the formic acid molecule, and occurring perpendicularly to the substrate surface (Bisschop et al. 2007a; Hellebust et al. 2007). These IR measurements describe the adsorption of HCOOH in its monomer and dimer forms. We observed a large IR band centering at 3200 cm^{-1} which corresponds to the OH stretching vibration mode $\nu_S(\text{O}-\text{H})$ of pure HCOOH and some H_2O molecules that come from the liquid aqueous phase. The presence of water is confirmed by the small IR band at 1620 cm^{-1} for the bending vibration mode $\nu_B(\text{HOH})$.

The RAIR spectrum b in Fig. 4 shows the significant decrease of the IR band at 1080 cm^{-1} to a greater than 80%, and the growth of new infrared absorption bands, mainly at 2342 cm^{-1} , 1535 cm^{-1} , and 1029 cm^{-1} . The IR band at 2342 cm^{-1} is attributed to the asymmetrical stretching vibration bond $\nu_S(\text{C}-\text{O})$ of CO_2 molecules, which at 1535 cm^{-1} is attributed to $\nu_S(\text{CH}_2)$ of H_2CO (Bouilloud et al. 2015), and the band at 1029 cm^{-1} to the stretching vibration mode $\nu_S(\text{C}-\text{O})$ of CH_3OH molecules (Martín-Doménech et al. 2014). These new species are likely to be formed by the reaction of HCOOH molecules with H atoms on the graphite surface at 10 K. However, the spectrum b does not show a noticeable decrease in the intensity of the main IR band of HCOOH at 1740 cm^{-1} after 50 min of H atom addition to HCOOH film, probably because the $\nu_S(\text{C}=\text{O})$ mode of HCOOH ice not consumed by H atoms overlaps with the $\nu_S(\text{C}=\text{O})$ mode of H_2CO molecules newly formed by the reaction $\text{HCOOH}+\text{H}$. Moreover, the widening of the IR band at 1740 cm^{-1} of the HCOOH in the spectrum b can be explained by the formation of HCOOH- H_2O complex between the HCOOH molecules adsorbed on the surface and the neighboring H_2O molecules formed by the reaction $\text{HCOOH}+\text{H}$ on the surface. These newly formed H_2O molecules are identified by their absorption bending mode $\nu_B(\text{HOH})$ at about 1680 cm^{-1} (Bisschop et al. 2007a; Bouilloud et al. 2015) as a shoulder in the main absorption band of HCOOH. In the same spectrum b of Fig. 4, we observe an increase in the intensity of the large $\nu_S(\text{O}-\text{H})$ band at 3200–3500 cm^{-1} , which may correspond to HCOOH ice mixed with CH_3OH and H_2O newly formed on the surface. The RAIR spectra of pure HCOOH and HCOOH+H films in Fig. 4 show a very small IR feature at 2149 cm^{-1} with very low absorbance value ($<10^{-4}$), which may be attributed to background gaseous CO degassing from the cryocooler, and then accumulated on the surface during the deposition phase of HCOOH at 10 K. The intensity of this IR peak in spectrum b of Fig. 4 does not change significantly after H-atom bombardment of the HCOOH film. The infrared wave numbers of HCOOH and HCOOH+H systems found in this work on the graphite surface are summarized in Table 1.

Figure 5 shows the TPD curves of some masses for pure HCOOH ice (in black) and HCOOH+H system (in red) on HOPG surface. In Fig. 5a, we observe a decrease in the TPD peak of the HCOOH multilayer (m/z 46) centering at 159 K and a shift to 148 K after H-exposure, probably due to presence of water ice on the surface during the exposure phase. In parallel, in Fig. 5b we see the growth of a desorption peak at 82 K for the film of HCOOH+H, which may correspond to the desorption of CO_2 molecules formed by the reaction of HCOOH with H on the surface. The growth of the desorption of CO_2 correlates with

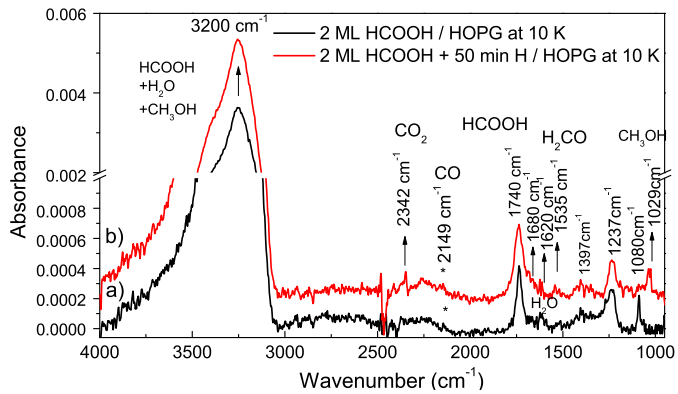


Fig. 4. RAIRS spectra of HCOOH and HCOOH + H films on HOPG surface using two beam lines. (a) RAIR spectrum of 2 ML HCOOH ice on graphite (HOPG) surface at 10 K; (b) RAIR spectrum of (2 ML HCOOH + 50 min H atoms) system on graphite (HOPG) surface at 10 K.

the small IR absorption band at 2342 cm^{-1} observed in the RAIR spectrum b of Fig. 4 at 10 K for the HCOOH+H film. In addition, Fig. 5 panels c and d show the growth of two TPD peaks centering at 143 K for masses m/z 32 and m/z 30, which are likely to be assigned to CH_3OH and H_2CO formed by the reaction of HCOOH+H, respectively. In Fig. 5e, we observe the growth of a TPD peak of mass m/z 28 at 45 K after H atom addition to the HCOOH film, which may correspond to CO molecules formed by the reaction HCOOH + H and mixed with CO contaminant coming from the cryocooler. Figure 5f shows the growth of a TPD peak at 143 K for mass m/z 18, which likely to be attributed to H_2O ice formed by the HCOOH+H surface reaction.

It is noted that similar HCOOH+H experiments (not shown in this work) have been performed on a bare gold surface, firstly by depositing two layers of HCOOH ice at 10 K and then adding H atoms for 45 min using two beam lines. QMS-TPD results have shown a significant decrease in the intensities of the TPD peaks of masses m/z 47 and m/z 46 of HCOOH by 40 and 60%, respectively after H beam addition to HCOOH pre-deposited film. However, despite the efficient consumption of HCOOH by H atoms on the gold surface, no detectable products except m/z 18 for H_2O molecules have been observed by TPD measurements in these experiments. The lack of products in these experiments can be explained by the effect of the chemical desorption of the products upon formation on the gold surface through the exothermic surface reactions.

3.3.2. HCOOH+H system on ASW ice surface

We performed similar HCOOH+H experiments on ASW ice surfaces. Figure 6 displays three RAIR spectra of HCOOH and HCOOH+H systems on an ASW ice: a an IR spectrum of pure 3 ML HCOOH ice on ASW ice surface at 10 K, b an IR spectrum of 3 ML HCOOH co-deposited simultaneously with H atoms during 11 min at 10 K, and c an IR spectrum with additional exposure time of H atoms for 120 min on the pre-deposited (HCOOH+H) film at 10 K. The RAIR spectrum a shows the absorption bands of pure HCOOH ice on the ASW ice surface at positions: 1070, 1216, 1394, 1729, 2589, 2743, 2934, and 3218 cm^{-1} . The labels and the vibrational modes of these IR peaks are given in Table 1. In this spectrum, we see a small redshift of the IR band at 1729 cm^{-1} with respect to that observed previously on graphite at 1740 cm^{-1} (Fig. 4, spectrum a). In the RAIR spectrum b of Fig. 6, we see the growth of a very

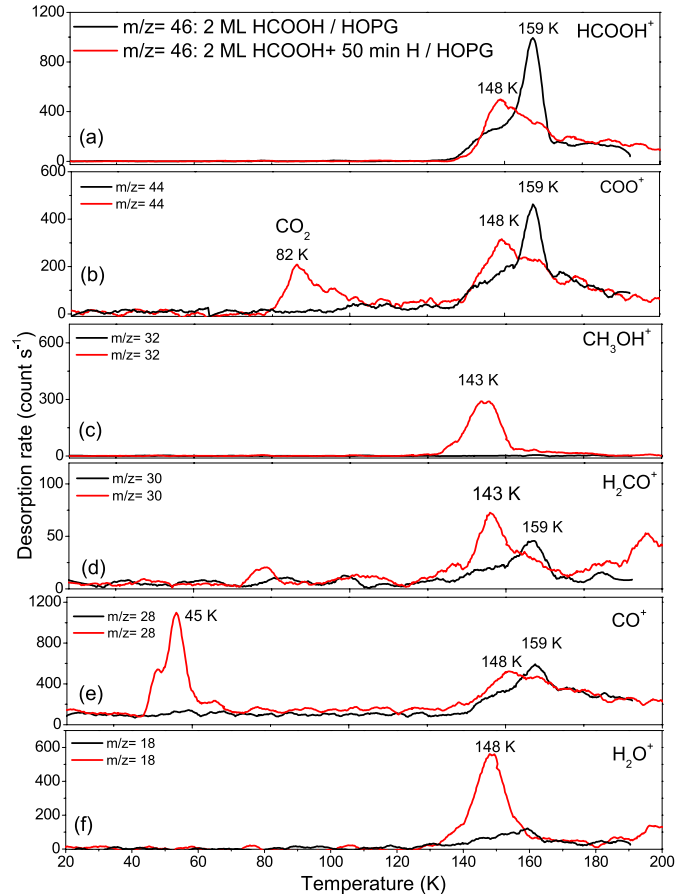


Fig. 5. TPD curves of HCOOH and HCOOH + H films on graphite (HOPG) surface for different masses. Black line: 2 ML of HCOOH ice on HOPG surface at 10 K; red line: 2 ML HCOOH + 50 min H atoms on HOPG surface at 10 K.

small IR peak at 2345 cm^{-1} during the first 11 min of HCOOH and H co-deposition on water ice surface at 10 K. This IR band that continues to grow with the additional H-exposure time for 120 min in the spectrum c is attributed to the stretching vibrational mode of CO_2 likely formed by the reaction HCOOH+H. The IR spectrum c also shows the disappearance of the peak at 1070 cm^{-1} for the bending (HCO) mode of HCOOH, and even the broadening and the increasing of the IR band at 1729 cm^{-1} . The broadening of the band could be affected by the bending mode $\nu_B(\text{HOH})$ of H_2O at about 1655 cm^{-1} , and the $\nu_S(\text{CH}_2)$ mode of H_2CO at about 1535 cm^{-1} (Bouilloud et al. 2015), which may be formed by the reaction HCOOH+H on the surface. The increase of the 1729 cm^{-1} IR band can be explained by the overlapping of the C=O stretching bond of H_2CO molecules (Bennett et al. 2011) with that of unreacted HCOOH. Spectrum c also shows the growth of two infrared bands at 1020 cm^{-1} and 3218 cm^{-1} with the increasing time of H atoms on the surface. The thin infrared absorption band at 1020 cm^{-1} is attributed to $\nu_S(\text{CO})$ mode of CH_3OH molecules (Bennett & Kaiser 2007), while the large infrared band at 3218 cm^{-1} is attributed to the stretching vibration mode OH of H_2O molecules mixed with HCOOH and CH_3OH species. In this experiment performed on ASW ice, RAIR spectra of pure HCOOH and HCOOH+H films on ASW ice in Fig. 6 don't show a clear IR band at around 2140 cm^{-1} for CO ice, but a large absorption band centered on 1997 cm^{-1} , which increases with H atom addition to HCOOH ice. This unexpected broad IR feature observed in RAIR spectra

Table 1. RAIR solid state spectral features for solid HCOOH and (HCOOH+H) observed in this work on graphite (HOPG) and np-ASW ice surfaces at 10 K.

Surface	Graphite	H ₂ O ice	Bond vibration	Assignment
	Wavenumber (cm ⁻¹)	Wavenumber (cm ⁻¹)		
HCOOH	1080	1070	$\nu_B(\text{HCO})^{(a),(b)}$ out-of-plane	HCOOH
	1237	1216	$\nu_S(\text{C-O})^{(a)}$	HCOOH
	1397	1394	$\delta(\text{OH})^{(c)}$; $\delta(\text{CH})^{(c),(g)}$	HCOOH
	1620		$\nu_B(\text{HOH})^{(a)}$	H ₂ O
	1740	1729	$\nu_S(\text{C=O})^{(a)}$	HCOOH
		1997		HCOO ⁺ + H ₃ O ⁺ ^(b)
	2149		$\nu_S(\text{OC})$	CO
		2589	$\nu_S(\text{OH})^{(a)}$	HCOOH
		2743	$\nu_S(\text{OH})^{(a)}$	HCOOH
		2934	$\nu_S(\text{CH})^{(a)}$	HCOOH
HCOOH+H	3200	3218	$\nu_S(\text{OH})^{(a)}$	HCOOH
	1029	1020	$\nu_S(\text{C-O})^{(d),(e)}$	CH ₃ OH
	1237	1216	$\nu_S(\text{C-O})^{(a)}$	HCOOH
	1397	1396	$\delta(\text{OH})^{(c)}$; $\delta(\text{CH})^{(c),(g)}$	HCOOH
	1535	1535	$\nu_S(\text{CH}_2)^{(c)}$	H ₂ CO
	1680	1655	$\nu_B(\text{HOH})^{(a),(c)}$	H ₂ O
	1740	1729	$\nu_S(\text{C=O})^{(a)}$	HCOOH, H ₂ CO
		1997		HCOO ⁺ + H ₃ O ⁺ ^(b)
	2149		$\nu_S(\text{OC})$	CO
	2342	2345	$\nu_S(\text{C=O})^{(f)}$	CO ₂
		2589	$\nu_S(\text{OH})^{(c)}$	HCOOH
		2743	$\nu_S(\text{OH})^{(c)}$	HCOOH
		2934	$\nu_S(\text{CH})^{(c)}$	HCOOH
	3200	3218	$\nu_S(\text{OH})^{(f)}$	HCOOH+H ₂ O + CH ₃ OH

Notes. ν_S refers to the symmetric and antisymmetric stretching mode, δ refers to antisymmetric deformation mode, ν_B refers to the bending mode (Bisschop et al. 2007b).

References. ^(a)Bisschop et al. (2007a); ^(b)Hellebust et al. (2007); ^(c)Bouilloud et al. (2015); ^(d)Bennett & Kaiser (2007); ^(e)Martín-Doménech et al. (2014); ^(f)Bennett et al. (2011); ^(g)Schutte et al. (1999).

a, b and c of Fig. 6 and increasing with H atom addition can result from the interaction of HCOOH with the water molecules of the substrate, according to the reference (Hellebust et al. 2007). In their work, the authors indeed observed a broad 2100–1900 cm⁻¹ feature centered on 2000 cm⁻¹ in their RAIR spectrum of thick mixed amorphous HCOOH and water ices at 110 K deposited on gold substrate. They attributed this IR absorption band to the presence of a small amount of oxonium H₃O⁺ and formate HCOO⁻ ions, indicating the ionization of the acid in a solid water matrix and not on the ice surface. For the authors, the ionization of formic acid is also evidenced by low frequency shoulder on the $\nu_S(\text{OH})$ mode of water band at 3220 cm⁻¹. The infrared wave numbers observed for HCOOH+H system on ASW ice are given in Table 1.

Figure 7 shows the TPD curves of 3 ML HCOOH pure ice (in black) and after exposure to H atoms (in red) on amorphous water ice. Figure 7, panels b and c show a 30% decrease in the intensities of the HCOOH multilayer TPD peaks of *m/z* 47 and *m/z* 46 at 147 K for HCOOH + H system with comparison to TPD peaks of pure HCOOH ice. This decrease indicates the consumption of HCOOH species by H atoms from the water ice surface. Whereas, TPD peaks at 158 K correspond to the fraction of formic acid co-desorbing with the crystalline water ice substrate. In parallel, we see the growth of a new TPD peak at 85 K for mass *m/z* 44 corresponding to CO₂ molecules

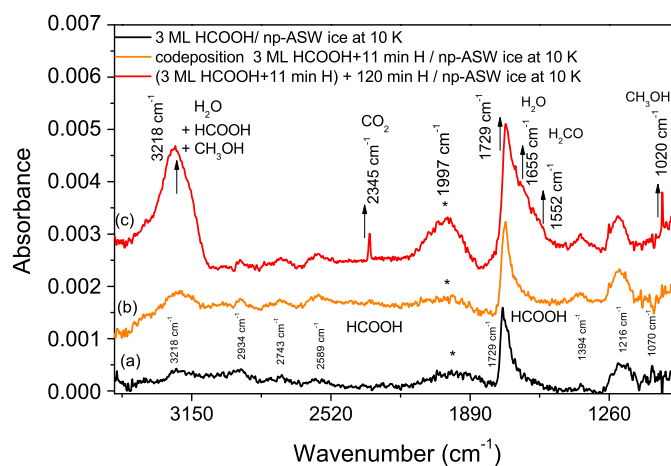


Fig. 6. RAIR spectra of HCOOH and HCOOH + H films on np-ASW of 10 ML thickness, deposited at 110 K and cooled down to 10 K. (a) 3 ML HCOOH on np-ASW ice surface at 10 K, (b) 3 ML HCOOH + 11 min H on np-ASW ice surface at 10 K, (c) (3 ML HCOOH + 11 min H) + 120 min H on np-ASW ice surface at 10 K.

likely formed by the reaction of HCOOH with H atoms, as has been previously observed by RAIR spectroscopy in Fig. 6, spectrum c.

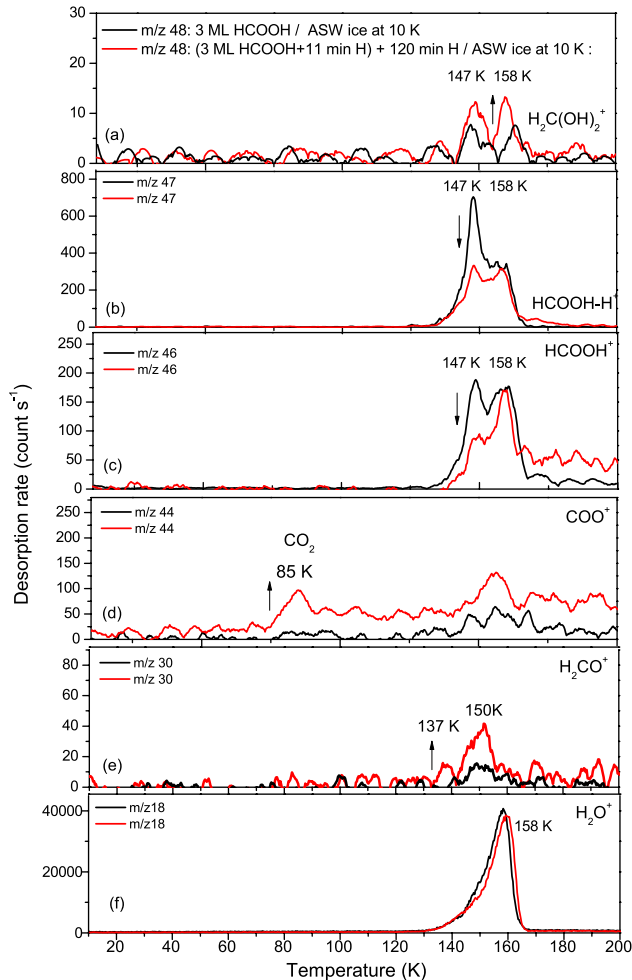


Fig. 7. TPD curves of HCOOH and HCOOH + H films on np-ASW ice surface for different masses from 10–200 K. Black line: 3 ML of HCOOH on 10 ML thickness of an ASW ice film prepared at 110 K and cooled down to 10 K, Red line: (3 ML HCOOH +11 min H) with an additional H atom bombardment of the film for 120 min on 10 ML thickness of an ASW ice film held at 10 K.

However, contrary to the previous experiment performed on graphite surface (Sect. 3.3.1), TPD curves of HCOOH+H on water ice did not show clear growth in the peaks of m/z 32, m/z 31 and m/z 30 at 120–150 K, corresponding to CO-bearing species (H_3COH , H_3CO , and H_2CO). In this TPD experiment on ASW ice, we did not observe a new TPD peak of m/z 32 at 120 K–150 K, which could correlate with the IR band at 1020 cm^{-1} , observed in the spectrum c of Fig. 6. Moreover, we observe the growth of small TPD peaks at 137 and 150 K for m/z 30 of the system (2 ML HCOOH +130 min H) in Fig. 6e, which may correspond to the cracking pattern H_2CO^+ . In addition, we observe the increase of two TPD peaks of m/z 48 at 148 K and 158 K in Fig. 7, panel a after H addition to the HCOOH film, which may correspond to the desorption of diol ($\text{H}_2\text{C}(\text{OH})_2$), m/z 48, formed by the reaction of HCOOH_2 radicals (m/z 47) with H atoms both on the surface and in the bulk of the water ice film.

3.3.3. Kinetic of (HCOOH + H) on ASW ice

Figure 8 shows the kinetic evolution of HCOOH and CO_2 present on the surface as a function of the co-deposition time of HCOOH and H atoms on the amorphous water ice surface held at 10 K.

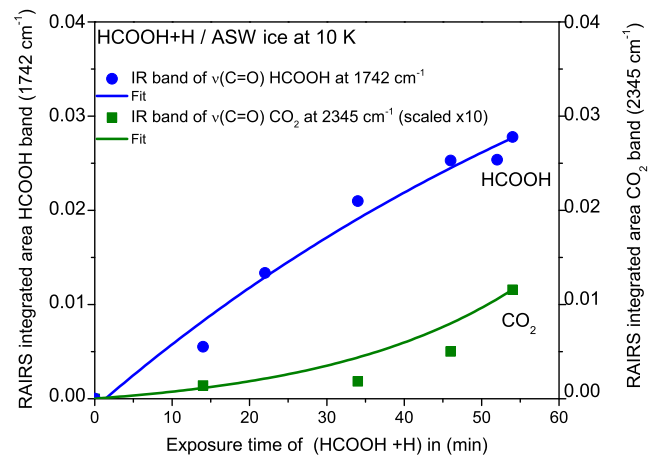


Fig. 8. Kinetic evolution of (HCOOH+H) system as a function of the exposure time (in s) of HCOOH and H beams on the ASW ice surface. The water ice film of 10 ML thickness is grown at 110 K, and cooled down to 10 K. The data are derived from the integrated areas below the RAIRS absorption bands of HCOOH and CO_2 at 1729 cm^{-1} and 2345 cm^{-1} , respectively.

These data correspond to the integrated areas below the RAIRS bands of HCOOH ice at 1729 cm^{-1} and that of CO_2 ice at 2345 cm^{-1} , measured during the simultaneous deposition phase of HCOOH and H on the ASW ice substrate. The experimental data of CO_2 are scaled by a factor of 10 to be observed in Fig. 8. We see the exponential growth of the HCOOH film and the slow increase in the amount of CO_2 on the surface with the exposure time of HCOOH and H beams during 55-min periods. These kinetics indicate the slow hydrogenation reaction of solid HCOOH by H atoms on the water ice at low surface temperature 10 K, probably caused by the high activation energy barriers of the hydrogenation reactions.

4. Discussion

Our present experiments performed in the sub-monolayer regime of 1–3 ML showed that the reactivity of HCOOH with H atoms at low surface temperature (10 K) depends on the substrate used in this work (graphite HOPG and ASW ice). The main products formed by the reaction HCOOH+H on the graphite surface, and observed by RAIRS and TPD are CO, H_2CO , CH_3OH , and H_2O . While in the case of the ASW ice surface, the main product formation identified by RAIRS and TPD is CO_2 . Our results contradict the experimental results of the Leiden group (Bisschop et al. 2007b) for the inefficient hydrogenation reaction of HCOOH with H atoms in the multilayer regime. In their work (Bisschop et al. 2007b), the authors bombarded thick (20 ML) pure HCOOH films covering gold substrate at surface temperature 12 K, using two H-fluxes of $7.8 \times 10^{13}\text{ atom cm}^{-2}\text{ s}^{-1}$ and $5.2 \times 10^{14}\text{ atom cm}^{-2}\text{ s}^{-1}$, which are 10–100 orders of magnitude higher than our current fluxes. The hydrogenations were performed under UHV conditions in which less than a monolayer of background gas is accreted during the timescale of the experiments. In their two difference RAIRS spectra for $\nu_s(\text{C}=\text{O})$ stretch, obtained between pure HCOOH and HCOOH+H ices spectra, recorded at two H atom deposition temperatures of 12 K and 40 K, they observed a small decrease (<0.1 ML) on the blue side of the stretching mode at 1710 cm^{-1} of HCOOH (seen at 1750 cm^{-1}) and an increase of a peak at 1730 cm^{-1} . They explained their IR observations by a slight change in the profile of the HCOOH band due to some restructuring of

the HCOOH ice surface by H bombardment. Because of the lack of new IR bands at 1500 cm^{-1} , in their difference spectra, they did not attribute the band at 1730 cm^{-1} to $\nu_S(\text{C}=\text{O})$ mode of H_2CO species. They also considered the measured low level of H_2CO formation observed in their experiment to have originated from the hydrogenation of background gaseous CO that is accreted on the surface during the experiments. Their CO contamination resulting from the degassing of the metal parts, was observed by an increase in the TPD signal of mass 28. In addition, in their TPD hydrogenation experiments, the authors did not detect masses 48 ($\text{CH}_2(\text{OH})_2$), 32 (CH_3OH), 31 (H_3CO) and 30 (H_2CO), and thus confirmed the inefficient reaction of $\text{HCOOH}+\text{H}$ in the ice at 12 K. The nondetection of $\text{CH}_2(\text{OH})_2$ in their experiment disagrees with our TPD results performed on water ice in the sub-monolayer coverage, clearly showing the desorption peak of mass 48 both from pure HCOOH and ($\text{HCOOH}+\text{H}$) systems at 148 K. This desorption peak is likely attributed in our experiments to the cracking pattern HCOOH_2^+ of HCOOH dimers in the head of the QMS for pure HCOOH ice, and to the reaction product ($\text{CH}_2(\text{OH})_2$) of H atom with the energetically stable radical HCOOH_2^* expected to be formed on the water ice. The authors also confirmed the non efficiency of formic acid hydrogenation by the high classical activation barrier (2.4 eV) of the $\text{HCOOH}+2\text{H} \rightarrow \text{H}_2\text{CO}+\text{H}_2\text{O}$ reaction in the ice, but they did not check the efficiency of the hydrogenation reaction by tunneling process using the isotopic species rich in a deuterium element. In both sub-monolayer and multilayer regimes, the hydrogenation reaction of HCOOH competes with the H+H barrierless recombination reaction leading to H_2 formation (Amiaud et al. 2007). In the work of the Leiden group (Bisschop et al. 2007b), the H atom mobility is likely to be reduced in the bulk of the ice, making hydrogenation reactions less efficient. While in our work, H atom diffusion on the surface sites is favored by the substrate of HOPG, which can itself be partially hydrogenated by the impinging hydrogen atoms. In this case, the presence of H_2 molecules already adsorbed on the surface of HOPG at 10 K may increase the sticking coefficient and the residence time of hydrogen atoms on the surface (Amiaud et al. 2007), favoring therefore its reaction either with another adsorbed H atom or with a neighboring condensed HCOOH molecule. In our experiments, we evaluated a consumption of 20–30% of formic acid by comparing the TPDs curves at m/z 46 of pure and H-exposed HCOOH ice. Our RAIR spectra show that the peak at 1080 cm^{-1} (1070 cm^{-1}) in spectrum a of Fig. 4 and Fig. 6 is significantly reduced after H atom bombardment. This peak attributed to the bending vibration mode $\nu_B(\text{HCO})$ of HCOOH molecules is the only peak that disappears in RAIR data, probably because it does not overlap with any vibration modes of other molecules (CH_3OH , H_2CO , CO , H_2O , and CO_2) observed in these experiments, contrary to the stretching mode $\nu_S(\text{C}=\text{O})$ at 1740 cm^{-1} (1729 cm^{-1}) of HCOOH, which overlaps with that of H_2CO at 1730 cm^{-1} , and even with $\nu_B(\text{HOH})$ mode of H_2O at about 1655 cm^{-1} .

Here, we propose a chemical routes for the reaction $\text{HCOOH}+\text{H}$ to explain the products formation observed in this work.

Formation of H_2O from $\text{HCOOH}+\text{H}$ system. The surface chemical process for the formation of H_2O molecules through the reaction $\text{HCOOH}+\text{H}$ involving the monomer HCOOH, is described by the reaction (5) of the H atom with the oxygen atom O of the hydroxyl group $-(\text{OH})$ of HCOOH. This OH-abstraction reaction reported in the work of Cao et al. (2014) produces a $\text{HCO}\dots\text{H}_2\text{O}$ complex after the breaking of a C–O bond and the

formation of a new H–O bond:



The formyl radical (HCO) has not been identified in our HCOOH+H experiments, neither in RAIR spectra at around 1860 cm^{-1} (Milligan & Jacox 1964), nor in TPD curves at a desorption temperature different from that of the cracking pattern (m/z 29) of HCOOH at around 148 K.

Formation of CO , H_2CO , CH_3OH from $\text{HCOOH}+\text{H}$ system. The H-addition to the radical (HCO) may form the formaldehyde (H_2CO), m/z 30 (identified by TPD and RAIRS on graphite), through the barrierless reaction (6) reported in Watanabe et al. (2003):



Newly formed H_2CO species can be hydrogenated by additional exposure time of H atoms to form methoxy (H_3CO) or (H_2COH), m/z 31, through the reaction (7):



and further successive H addition leads to the formation of saturated methanol (CH_3OH), m/z 32 (identified by TPD and RAIRS on graphite), through the barrierless reaction (8):

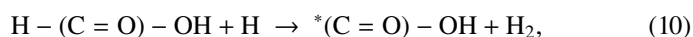


The successive hydrogenation reactions of HCO, H_2CO , and H_3CO ices by H atoms on cold surfaces have been demonstrated experimentally (Watanabe et al. 2003; Watanabe & Kouchi 2002) by the exposure of CO ices to room temperature hydrogen atoms generated from a microwave-induced plasma. However, since Fig. 5, panel e in Sect. 3.3.1 shows an increase in the TPD peak of m/z 28 at 45 K for the system ($\text{HCOOH}+\text{H}$) deposited on the graphite surface, we suggested that CO can also be formed by the exothermic abstraction reaction (9) between HCO and H atoms on the surface (Minissale et al. 2016b) as follows:



Furthermore, the CO ice present on the surface at 10 K can in turn undergo successive H-addition reactions leading to the formation of CO-bearing ices (from HCO to CH_3OH) as reported in many studies (Watanabe et al. 2003; Minissale et al. 2016b; Chuang et al. 2018).

Formation of CO_2 from $\text{HCOOH}+\text{H}$ system. The formation of the CO_2 from the $\text{HCOOH}+\text{H}$ reaction may result from the H-abstraction reaction (10) occurring on the carbon atom of the HCOOH molecule, followed by the H-addition reaction (11) to the formate radical $^*\text{COOH}$, leading to the ejection of H atom and the breaking of an O–H bond. The reaction (11) is exothermic with a standard enthalpy of formation $\Delta H = -72.3\text{ kJ mol}^{-1}$ or -8232.2 K (Jiang et al. 2017):



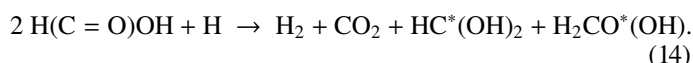
The reaction (11) is demonstrated theoretically by DFT calculation with a high energy barrier of 1.74 eV (Jiang et al. 2017). Moreover, the abstraction of H atom from the hydroxyl (O–H) bond of HCOOH molecules may lead to the radical $\text{H}(\text{C}=\text{O})\text{O}^*$ through the reaction (12):



The H-addition reaction (13) to $\text{H}(\text{C}=\text{O})\text{O}^*$ may form CO_2 after the breaking of a C–H bond. This exothermic reaction (13) with a standard enthalpy of formation $\Delta H = -26.0 \text{ kJ mol}^{-1}$ or -3133.2 K is also evidenced by a DFT calculation with a high energy barrier of 1.97 eV (Jiang et al. 2017):

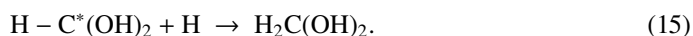


The high activation energy barriers of the H-abstraction reactions (11) and (13) make the production of CO_2 from $\text{HCOOH}+\text{H}$ reaction difficult through the monomer HCOOH . So, it is likely that the hydrogenation of HCOOH dimers contribute to the formation of CO_2 molecules on the surface through the exothermic reaction (14). This reaction may in-turn dissociate $\text{HCOOH}-\text{HCOOH}$ condensates into CO_2 (m/z 44), and two possible radicals $\text{HC}^*(\text{OH})_2$ and $\text{H}_2\text{CO}^*(\text{OH})$ (m/z 47) (Cao et al. 2014), therefore producing H_2 molecules by the abstraction of a H atom from C–H bond of HCOOH and the cleavage of O–H and C–H bonds:



The energy of the hydrogenation reaction (14) is $\Delta H_r = -14 \text{ kJ mol}^{-1}$ or -1680 K , calculated from the standard heats of formation available on the NIST WebBook.

In the case of the water ice experiments, the energetically favorable radical $\text{HC}^*(\text{OH})_2$ (Cao et al. 2014) may be stabilized by the water ice environment and the hydrogen bonding with the neighboring H_2O molecules. Its hydrogenation by H atom through the reaction (15) forms the diol $\text{H}_2\text{C}(\text{OH})_2$ (m/z 48). This reaction explains well our previous $\text{HCOOH}+\text{H}$ results on ASW ice (Sect. 3.3.2, Fig. 7) for the decrease of the TPD peak of m/z 47 at 147 K, and the increase of the TPD peaks of m/z 48:



The proposed chemical reaction routes for the $\text{HCOOH}+\text{H}$ system are illustrated in Fig. 9. The reaction pathway involving the dimer of HCOOH to explain the formation of CO_2 and the diol $\text{H}_2\text{C}(\text{OH})_2$ on an ASW ice surface is a hypothesis that needs to be confirmed by further experiments with the deuterated species of formic acid and new theoretical works.

The fact that CO , H_2CO and CH_3OH are not formed in HCOOH on ASW means that the abstraction of the OH group from HCOOH is less favorable on water ice. This is probably because the OH functional groups of adsorbed HCOOH monomers are involved either in the formation of hydrogen bonds with the H_2O molecules of the water ice, or in the formation of dimers ($\text{HCOOH}-\text{HCOOH}$) through hydrogen bonding. However, the water ice substrate may play an important role in reducing the height of the activation barriers of the exothermic H-abstraction reactions (10–13), by dissipating the excess energy of the reaction to the water ice, therefore favoring the formation of CO_2 molecules rather to CO bearing species. This leads us to believe that the -OH group of HCOOH is likely to be oriented towards the H_2O molecules of the ice. While in the case of HOPG substrate, the HCOOH is strongly adsorbed on the surface with a specific orientation that forbids the H-abstraction reaction from the $\text{H}-(\text{CO})\dots$ side of the molecule.

In the hydrogenation experiments of Bisschop et al. (2007b), the authors suggested that other reactive products, such as hydroxyl OH radicals are also formed by photolysis of H_2O molecules, making the discrimination of different effects difficult. In our hydrogenation experiments performed in the submonolayer regime, some OH radicals can be created within the

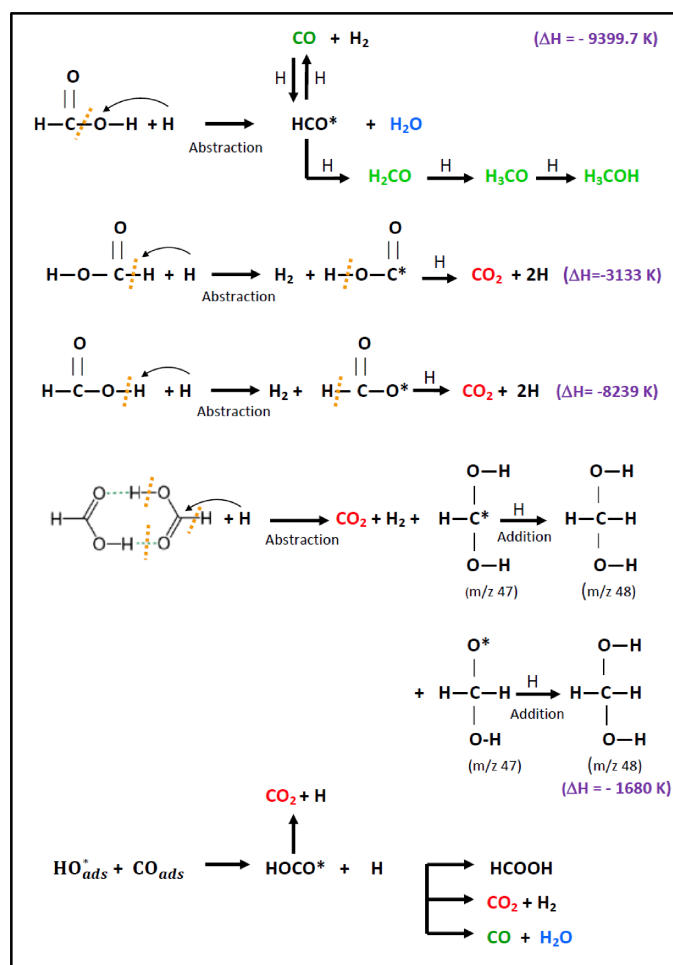


Fig. 9. Chemical reaction routes for the hydrogenation $\text{HCOOH}+\text{H}$ reaction on cold graphite (HOPG) and ASW ice surfaces involving monomer and dimer of formic acid.

microwave-induced plasma via the impact of some energetic photons to HCOOH , H_2O ices and/or HOPG substrate, during the running of the hydrogen source, therefore forming some hydrocarboxyl (HOCO) complexes with traces of adsorbed CO species following the reaction (16):



In their computational DFT studies on carbonaceous surface, Goumans et al. (2008) reported that the stabilized adsorbed HOCO intermediate via intramolecular energy transfer to the surface can either yield $\text{CO}_2 + \text{H}$ through the reaction (17):



or react in a barrierless process with an additional H atom to form back HCOOH , following reaction (18), or $\text{CO}_2 + \text{H}_2$ and $\text{CO} + \text{H}_2\text{O}$ ices (reactions 19 and 20):



These three pairs of products depend on the orientation of the HOCO and the incoming hydrogen atom (Goumans et al. 2008).

The back hydrogenation into HCOOH can reduce the amount of other products (CO, formed going back to HCOOH), and therefore explain the increase of the IR stretching $\nu(\text{C}=\text{O})$ band at 1740 cm^{-1} of HCOOH observed in our experiments. Taking into account the possible HOCO chemical route in our work, the CO_2 observed in our (HCOOH+H) experiments as a main product can also be formed another way with the HO–CO complex as precursor. However, the identification of the radical OH and the HO–CO intermediate on the HOPG and water ice is not obvious through RAIR spectroscopy or even through TPD mass spectrometry measurements. Our RAIR spectra performed on the HOPG surface show that only the IR band at 1080 cm^{-1} for the bending mode (H–C–O) of HCOOH disappears during the hydrogenation of HCOOH ice. The decrease of this IR peak may result from the breaking of the H–C bond by H-abstraction reaction from H–C side of HCOOH molecule. If it is indeed the case, the H-abstraction will lead to the formation of $\text{H}_2 + \text{COOH}$ radical, rather to HCO radical + H_2O , after further hydrogenation. This hypothesis cannot explain our CO-bearing species (H_2CO , H_3CO , CH_3OH , and CO) observed by RAIRS and TPD on HOPG, because these species are formed by successive hydrogenation (or dehydrogenation) of a HCO radical, which is produced by the OH-abstraction reaction (5) of HCOOH by H atom and the breaking of the O–C bond. However, since there are traces of CO deposits on the surface, the IR band at 1080 cm^{-1} can be assigned both to $\nu_{\text{B}}(\text{HCO})$ vibrational mode of HCOOH and to another C–O stretching vibrational fundamental of the cis (or trans) HO–CO intermediate (Milligan & Jacox 1971), probably formed on the surface from traces of OH and CO on the surface (Goumans et al. 2008). In this case, the hydrogenation of HCOOH and HOCO may explain the disappearance of the IR absorption band at 1080 cm^{-1} in the spectrum b of Fig. 4, and therefore the partial (20–30%) consumption yield of HCOOH estimated from TPD measurements. In our RAIR spectra of HCOOH+H, we did not observe IR peaks at 1833 , 1820 cm^{-1} , and even at 1796 , 1775 cm^{-1} characterizing trans-HOCO and cis-HOCO intermediates, respectively. IR bands of trans and cis-HOCO at 1833 and 1796 cm^{-1} were identified by Milligan & Jacox (1971) for the reaction of CO with OH in ices when performing vacuum-ultraviolet photolysis experiments of H_2O in a CO matrix at 14 K.

5. Astrophysical implications and conclusions

Formic acid is among the most common constituent of ices in star-forming and molecular cloud regions. Knez et al. (2005) (and references therein) have reported abundances of between two and ten with respect to water. HCOOH plays a major role in the formation of complex organic molecules in interstellar ices due to the reactions with H-atoms. In this paper, we experimentally demonstrate, through TP-DED mass spectrometry, the dimerization of HCOOH molecules on cold surfaces at temperatures of 10–100 K, and their possible implication in the reactivity of HCOOH with H atoms on graphite and ASW ice. The HCOOH+H reaction is likely to be enhanced by the mobility of atomic hydrogen at 10 K (Matar et al. 2008), which could induce bond cleavages C–H and O–H of HCOOH molecules. Our results indicate that formic acid molecules can be hydrogenated by H atom bombardment on interstellar ice subjected to ionizing radiation. The hydrogenation HCOOH+H reaction on HOPG and ASW ice surfaces leads to the dissociation of formic acid molecules and the formation of new species, such as CO_2 , H_2O , and CO-bearing species (from CO to CH_3OH), which are identified by RAIR and TPD spectroscopies. On the

other hand, we do not find any clear signature of COMs (except for methanol) formed via HCOOH hydrogenation. However, some CO-bearing products are subject to reactive desorption through the exothermic hydrogen-abstraction surface reactions, as has been demonstrated in previous laboratory experiments (Chuang et al. 2018; Minissale et al. 2016b), astrochemical models (Vasyunin & Herbst 2013), and recent theoretical studies (Morisset et al. 2019). This chemical desorption effect (Dulieu et al. 2013) should be taken into account in the evaluation of the product formation of the hydrogenation HCOOH+H reaction, in addition to other factors, such as the molecular ice environment that can stabilize some intermediates (HCOOH_2^* , HCOO^* , $^*\text{COOH}$, HO–CO*), and even the geometrical orientations of the dissymmetrical HCOOH molecules and their conformers (cis and trans) toward specific directions favoring or enabling H/OH abstraction surface reactions.

In our experiments, we evaluated a consumption of 20–30% of formic acid by comparing the TPD curves at m/z 46 of pure and H-exposed HCOOH ices. By considering that we exposed pure HCOOH films to a total H-atom fluence of $3 \times 10^{16}\text{ atom cm}^{-2}$, it means that only 10% of adsorbed hydrogen atoms react with HCOOH molecules in our experimental conditions. We stress that such a small H-atom fraction strongly depend both on HCOOH+H activation energy barrier and surface recombination of H atoms. For lower H-atom flux (i.e., in conditions similar to those encountered in interstellar ice) the rate of H-atom recombination would decrease with a simultaneous increase of the HCOOH+H reaction rate. Unfortunately, due to the presence of overlapping IR signatures (especially in the 1700 cm^{-1} region), RAIR spectra cannot be used to study the kinetics of HCOOH+H reaction, and thus to evaluate the activation barrier of the reaction. For this concern, further experiments with deuterium isotopic species are required to study the kinetics of the hydrogenation and the deuteration reactions. However, with the H-atom fluence actually used, the hydrogenation reaction of the smallest acid compound (HCOOH) seems to be efficient on water ice (30%), but slower than other hydrogenation reactions (O+H) (50%) (Dulieu et al. 2010), and ($\text{O}_3 + \text{H}$) (>50%) (Mokrane et al. 2009) leading to water ice formation. In this work, we also demonstrated the production of astrophysical relevant species CO_2 , H_2O by hydrogenation of HCOOH ices. The formation of CO_2 through the successive H-abstraction reactions (10–13) of HCOOH (Jiang et al. 2017) is favored by the water ice substrate. This result has a great importance in the solid phase chemical composition of icy mantles in star-forming regions. However, the spectroscopy of the main ice constituents, such as carboxylic acids should be better understood, with the new infrared observations in the interstellar ices by James Webb Space Telescope (JWST). Our hydrogenation reactions of HCOOH on cold grain surfaces may help astrophysicists and astrochemists to further understand the chemistry in gas-grain interfaces of protoplanetary disk regions, where gaseous molecules CO, CH_3OH , and HCOOH are expected to be abundant according to the recent astrochemical models of Ruaud & Gorti (2019). These species are likely to be formed on grain surfaces via hydrogenation reactions and then desorb into the gas phase, either through a chemical desorption process in the outer midplane disk cold regions ($T < 15\text{ K}$) located at higher vertical column densities ($A_{\text{V}} > 10\text{ mag}$), or via the photoprocessing of ices in disk midplane regions at $3 < A_{\text{V}} < 10\text{ mag}$ (Ruaud & Gorti 2019). These astrophysical environments are believed to be birthplaces of planetary systems and comets.

Acknowledgements. This work was supported by the Programme National Physique et Chimie du Milieu Interstellaire (PCMI) of CNRS/INSU with

INC/INP co-funded by CEA and CNES. The authors sincerely thank the anonymous referee for his powerful and helpful comments.

References

- Amiaud, L., Dulieu, F., Fillion, J.-H., Momeni, A., & Lemaire, J. L. 2007, *J. Chem. Phys.*, **127**, 144709
- Bennett, C. J., & Kaiser, R. I. 2007, *ApJ*, **660**, 1289
- Bennett, C. J., Hama, T., Kim, Y. S., Kawasaki, M., & Kaiser, R. I. 2011, *ApJ*, **727**, 27
- Bisschop, S. E., Fuchs, G. W., Boogert, A. C. A., van Dishoeck, E. F., & Linnartz, H. 2007a, *A&A*, **470**, 749
- Bisschop, S. E., Fuchs, G. W., van Dishoeck, E. F., & Linnartz, H. 2007b, *A&A*, **474**, 1061
- Bouilloud, M., Fray, N., Bénilan, Y., et al. 2015, *MNRAS*, **451**, 2145
- Burke, D. J., Puletti, F., Brown, W. A., et al. 2015, *MNRAS*, **447**, 1444
- Cao, Q., Berski, S., Debout, Z., Räsänen, M., & Khriachtchev, L. 2014, *Phys. Chem. Chem. Phys.*, **16**, 5993
- Chaabouni, H., Diana, S., Nguyen, T., & Dulieu, F. 2018, *A&A*, **612**, A47
- Chuang, K. J., Fedoseev, G., Qasim, D., et al. 2018, *ApJ*, **853**, 102
- Congiu, E., Chaabouni, H., Laffon, C., et al. 2012, *J. Chem. Phys.*, **137**, 054713
- Dulieu, F., Amiaud, L., Congiu, E., et al. 2010, *A&A*, **512**, A30
- Dulieu, F., Congiu, E., Noble, J., et al. 2013, *Sci. Rep.*, **3**, 1338
- Favre, C., Fedele, D., Semenov, D., et al. 2018, *ApJ*, **862**, L2
- Garrod, R. T., Widicus Weaver, S. L., & Herbst, E. 2008, *ApJ*, **682**, 283
- Goumans, T. P. M., Uppal, M. A., & Brown, W. A. 2008, *MNRAS*, **384**, 1158
- Hellebust, S., O’Riordan, B., & Sodeau, J. 2007, *J. Chem. Phys.*, **126**, 084702
- Henderson, G. 1987, *J. Chem. Edu.*, **64**, 88
- Ioppolo, S., Cuppen, H. M., van Dishoeck, E. F., & Linnartz, H. 2011, *MNRAS*, **410**, 1089
- Irvine, W. M., Friberg, P., Kaifu, N., et al. 1990, *A&A*, **229**, L9
- Jiang, Z., Qin, P., & Fang, T. 2017, *Appl. Surf. Sci.*, **396**, 857
- Keane, J. V., Tielens, A. G. G. M., Boogert, A. C. A., Schutte, W. A., & Whittet, D. C. B. 2001, *A&A*, **376**, 254
- Knez, C., Boogert, A. C. A., Pontoppidan, K. M., et al. 2005, *ApJ*, **635**, L145
- Lefloch, B., Ceccarelli, C., Codella, C., et al. 2017, *MNRAS*, **469**, L73
- Liu, S.-Y., Mehringer, D. M., & Snyder, L. E. 2001, *ApJ*, **552**, 654
- Lopes, S., Fausto, R., & Khriachtchev, L. 2018, *J. Chem. Phys.*, **148**, 034301
- Makochekanwa, C., Bankovic, A., Tattersall, W., et al. 2014, *A&A*, **566**, L5
- Martín-Doménech, R., Mu noz Caro, G. M., Bueno, J., & Goesmann, F. 2014, *A&A*, **564**, A8
- Matar, E., Congiu, E., Dulieu, F., Momeni, A., & Lemaire, J. L. 2008, *A&A*, **492**, L17
- Milligan, D. E., & Jacox, M. E. 1964, *ApJ*, **41**, 3032
- Milligan, D. E., & Jacox, M. E. 1971, *J. Chem. Phys.*, **54**, 927
- Minissale, M., Congiu, E., & Dulieu, F. 2016a, *A&A*, **585**, A146
- Minissale, M., Moudens, A., Baouche, S., Chaabouni, H., & Dulieu, F. 2016b, *MNRAS*, **458**, 2953
- Minissale, M., Nguyen, T., & Dulieu, F. 2019, *A&A*, **622**, A148
- Mokrane, H., Chaabouni, H., Accolla, M., et al. 2009, *ApJ*, **705**, L195
- Morisset, S., Rougeau, N., & Teillet-Billy, D. 2019, *Mol. Astrophys.*, **14**, 1
- Nguyen, T., Baouche, S., Congiu, E., et al. 2018, *A&A*, **619**, A111
- Noble, J. A., Congiu, E., Dulieu, F., & Fraser, H. J. 2012, *MNRAS*, **421**, 768
- Pilling, S., Baptista, L., Boechat-Roberty, H. M., & Andrade, D. P. P. 2011, *Astrobiology*, **11**, 883
- Ruud, M., & Gorti, U. 2019, *ApJ*, **885**, 146
- Schutte, W. A., Boogert, A. C. A., Tielens, A. G. G. M., et al. 1999, *A&A*, **343**, 966
- Skouteris, D., Balucani, N., Ceccarelli, C., et al. 2018, *ApJ*, **854**, 135
- Szymafiski, M., & Gillan, M. 1996, *Surf. Sci.*, **367**, 135
- Vastel, C., Ceccarelli, C., Lefloch, B., & Bachiller, R. 2014, *ApJ*, **795**, L2
- Vasyunin, A. I., & Herbst, E. 2013, *ApJ*, **769**, 34
- Vasyunin, A. I., Caselli, P., Dulieu, F., & Jiménez-Serra, I. 2017, *ApJ*, **842**, 33
- Watanabe, N., & Kouchi, A. 2002, *ApJ*, **571**, L173
- Watanabe, N., Shiraki, T., & Kouchi, A. 2003, *ApJ*, **588**, L121
- Woods, R. C., Gudeman, C. S., Dickman, R. L., et al. 1983, *ApJ*, **270**, 583